Optical Engineering

OpticalEngineering.SPIEDigitalLibrary.org

Fast tracking of wind speed with a differential absorption LiDAR system: first results of an experimental campaign at Stromboli volcano

Stefano Parracino
Simone Santoro
Giovanni Maio
Marcello Nuvoli
Alessandro Aiuppa
Luca Fiorani

SPIE.

Stefano Parracino, Simone Santoro, Giovanni Maio, Marcello Nuvoli, Alessandro Aiuppa, Luca Fiorani, "Fast tracking of wind speed with a differential absorption LiDAR system: first results of an experimental campaign at Stromboli volcano," *Opt. Eng.* **56**(4), 044104 (2017), doi: 10.1117/1.OE.56.4.044104.

Fast tracking of wind speed with a differential absorption LiDAR system: first results of an experimental campaign at Stromboli volcano

Stefano Parracino,[a,b,*] Simone Santoro,[b,c] Giovanni Maio,[b,d] Marcello Nuvoli,[e] Alessandro Aiuppa,[c] and Luca Fiorani[e]
[a]University of Rome Tor Vergata, Department of Industrial Engineering, Rome, Italy
[b]ENEA Guest, Frascati (RM), Italy
[c]University of Palermo, Department of Earth and Sea Sciences, Piazza Marina, Palermo, Italy
[d]Vitrociset S.p.A., Via Tiburtina, Rome, Italy
[e]ENEA, Fusion and Technology for Nuclear Safety and Security Department, Frascati (RM), Italy

Abstract. Carbon dioxide (CO_2) is considered a precursor gas of volcanic eruptions by volcanologists. Monitoring the anomalous release of this parameter, we can retrieve useful information for the mitigation of volcanic hazards, such as for air traffic security. From a dataset collected during the Stromboli volcano field campaign, an assessment of the wind speed, in both horizontal and vertical paths, performing a fast tracking of this parameter was retrieved. This was determined with a newly designed shot-per-shot differential absorption LiDAR system operated in the near-infrared spectral region due to the simultaneous reconstruction of CO_2 concentrations and wind speeds, using the same sample of LiDAR returns. A correlation method was used for the wind speed retrieval in which the transport of the spatial inhomogeneities of the aerosol backscattering coefficient, along the optical path of the system, was analyzed. [DOI: 10.1117/1.OE.56.4.044104]

Keywords: volcanic hazard; LiDAR; differential absorption LiDAR; correlation; carbon dioxide; wind speed.

Paper 161637 received Oct. 20, 2016; accepted for publication Apr. 4, 2017; published online Apr. 18, 2017.

1 Introduction

Millions of people currently live in the proximity of active or quiescent volcanoes and, therefore, are potentially exposed to the deleterious effects of their eruptions. In fact, volcanic eruptions can create an increase in air pollution levels; they are able to influence climate changes[1] and, in some circumstances, to kill a large number of humans, destroy the adjacent environment, and cause serious damage to national/international economies.

Mitigation of these effects requires careful assessment of volcano behavior and activity, which can be accomplished via instrument-based volcano monitoring. Accurate knowledge of the gas composition in volcanic plumes gives information on the geophysical processes taking place inside volcanoes and provides alerts on possible eruptions.[2]

Until recently, coupled gas-geophysical studies were sparse due to the difference in their sampling frequency (low for gas data). This explains the interest of earth scientists in new techniques of gas detection, in particular for CO_2, the second most abundant gas in volcanic fluids and the most directly linked to "pre-eruptive" degassing processes.[2,3]

A new differential absorption LiDAR (DIAL) designed to measure the volcanic CO_2 flux was developed as part of the ERC Starting Grant Project "BRIDGE." The Bridge Volcanic LiDAR (BILLI), recently developed at ENEA Research Center of Frascati, successfully retrieved three-dimensional tomographic measurements of volcanic CO_2 in the plumes, at Italian volcanoes Pozzuoli Solfatara (Naples, Italy),[3–5] Stromboli volcano (Sicily, Italy),[6,7] and Mount Etna (Sicily, Italy).[8] To our knowledge, this was the first time that CO_2 in a volcanic plume was retrieved by LiDAR. BILLI opens unprecedented possibilities in measuring volcanic CO_2 concentrations in excess of a few tens of ppm that can be clearly resolved at a distance of $\geq$3 km with a spatial resolution of $\leq$5 m and temporal resolution of $\leq$10 s.

Quantifying the CO_2 output from Pozzuoli Solfatara and Stromboli was vital to interpreting—and possibly predicting—the future evolution of the volcanic system, yielding huge benefits to the population living nearby. These examples show the huge social values of LiDAR systems in monitoring gas emissions. Observations near densely populated volcanic regions will have a high societal impact throughout Europe.

Another field where eruption forecasting would be crucial is air traffic control. In fact, volcanic ash is a major hazard to aircraft.[9] Smoke and ash from eruptions reduce visibility for visual navigation, and microscopic debris in the ash can sandblast windscreens and melt in the heat of aircraft turbine engines, damaging engines and making them shut down.[9,10] The most famous example was the air travel disruption after the 2010 Eyjafjallajökull eruption in Iceland. After an initial uninterrupted shutdown over much of northern Europe from the April 15 to April 23, airspace was closed intermittently in different parts of Europe in the following weeks as the path of the ash cloud was tracked. The shutdown had an impact on the economy and cultural events across Europe. Air travel and transport throughout the world was cancelled due to the airspace restrictions, and the International Air Transport Association (IATA) estimated that the total loss for the airline industry was around €1.3 billion.[11] Similar events also took

*Address all correspondence to: Stefano Parracino, E-mail: stefano.parracino@uniroma2.it

0091-3286/2017/$25.00 © 2017 SPIE

place in the south of Italy, where the eruptions of Mount Etna caused the closing of the airports of Catania in 2011[12] and 2014,[13] and Reggio Calabria in 2015.[14]

Also in this case, LiDAR stations could provide a rapid alert to air traffic governing bodies, who could adopt appropriate countermeasures, such as boosting alternative air routes or rail transport, thus minimizing economic losses.

Since LiDARs can profile aerosols over large areas with high spatial resolution, they have the potential to map the spatial concentration of particulates as a function of time. The ability to track these spatial structures in time allows one to determine the wind speed.[15] The latter is a crucial parameter that should be taken into account to adopt effective countermeasures against the previously cited events.

In the case of volcanic particle transport toward airports or residential areas, the knowledge of the wind speed and direction could be of vital importance to local authorities. For the previous reasons, in this work, particular attention will be paid to the retrieval of wind speed in the proximity of an active volcanic region using the BILLI DIAL system.

The area chosen for our experiments was the Stromboli island, off the north coast of Sicily in Italy, which hosts one of the most active Italian volcanos. This volcano is characterized by a persistent eruptive activity (recent eruptions in 2003 and 2007 caused serious damage)[16,17] that can generate explosive convective clouds that reach heights of several kilometers.[18] Moreover, considering its strategic position in the Tyrrhenian Sea, in the proximity of the main Mediterranean southern air routes, continuous monitoring of this region is necessary and useful.

According to the literature,[15] the measurement of winds is a well-developed technique using elastic backscatter LiDARs. Because of the small physical size of the laser beam and the short pulse width of the laser, the potential exists for LiDARs to make wind measurements with higher spatial and temporal resolution than current sodars or radars. Today, scanning high spectral resolution LiDAR has taken the wind measurement via tracking aerosol/cloud to a high degree of sophistication.[19]

Currently, there are numerous valid scientific studies and methods to determine wind speed and direction as well as some turbulence parameters.[15] They are basically divided into coherent methods that rely on laser Doppler velocimetry[20] and incoherent methods.[21] Incoherent methods of wind measurement are not as widespread since they are not as accurate as conventional coherent methods, and they often require the use of relatively high pulse energies that are not eye safe and are generally considered to be inappropriate for routine measurements.[15]

Despite our shot-per-shot incoherent DIAL system being not as accurate as coherent methods, it has certain advantages compared with conventional incoherent systems. In fact, as will be shown in Sec. 2.1 of this paper, the laser source works in the IR-B region and the pulse energy is low, compared with previous works.[21,22] As a consequence, the system operates within the exposure limits imposed by European directive 2006/25/EC,[23] and it is eye-safe.

It should be noted that our system was not originally conceived for wind speed tracking but only for CO_2 concentration measurements. Since the knowledge of wind speed is fundamental also for CO_2 flux calculation,[5,7,8] it was considered useful to assess this parameter using only our LiDAR system, independent of conventional acquisitions.

Therefore, using the same sample of LiDAR returns, it provides accurate measures of in-plume CO_2 concentration and, despite the limitations in accuracy, it is also able to retrieve a fast tracking of wind speed directly *in-situ*, without changing the system setup and without additional costs, simply by means of a further computational effort that consists of an advanced data processing method reviewed here.

Here, a simple point correlation method was used for rapid prediction of wind speed evolution. It is basically an attempt to track the motion of discrete atmospheric structures by differences in their particulate backscatter. By tracking the displacement of spatial inhomogeneities of the aerosol backscattering coefficient along the optical path, it is possible to determine the wind speed.[21,22,24–26]

After a brief description of the system components and in field setup, the correlation methodology used in the data processing, inspired by the pioneering work of Eloranta (1975),[21] will be explained in further detail. Wind profiles from a significant dataset, acquired during the experimental campaign of Stromboli in June 2015, will be presented and discussed. The analysis and conclusions will show that the performance of our system has made it possible to build a methodology for the fast tracking of not only the CO_2 concentration and flux[3–8] but also the wind speed.

2 Materials and Methods

2.1 *BILLI System*

BILLI[3–8] is a complex DIAL system for environmental remote sensing that provides ground based and range resolved remote measurements of CO_2 concentrations via differential backscatter.

It is mounted in a 3.5-ton truck, usually positioned far from the volcanic plume, and probes the plume with a laser beam. Due to two large elliptical mirrors, the instrument field of view can be aimed in any direction. With such a configuration, which scans the plume in both horizontal and vertical planes, the CO_2 concentrations outside and inside the volcanic plume are measured. These measurements, once carried out over a significant part of the plume and upon scaling to the transport rate (as derived from the wind speed at the plume altitude), allow one to retrieve the carbon dioxide flux. More details about this procedure are reported in Refs. 5 and 6.

As already stated, such an established system can also be used for the measurement of wind speed[27–29] due to the ability of steering the optics in different directions. The number of photons backscattered by the atmosphere at a given distance from the instrument is proportional to the backscattering coefficient. This factor is a function of the density of aerosols responsible for the light scattering. Any change in its spatiotemporal distribution during a data acquisition, therefore, will lead to variations in the LiDAR returns from one laser shot to another. As will be shown in the next section, the wind speed can be obtained from the transport of the spatial inhomogeneities of the backscattering coefficient along the optical path.[27]

The system is composed of a transmitter and receiver equipment [Fig. 1(a)]. Due to two large elliptical mirrors, the instrument field of view can be aimed at any direction within a large field of regard [Fig. 1(b)].

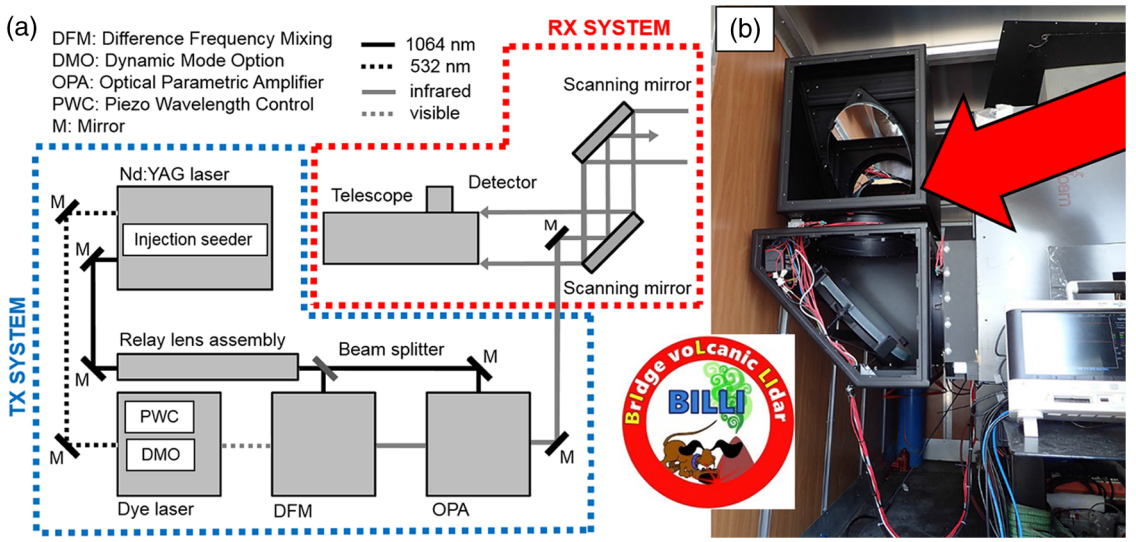

Fig. 1 (a) Technical scheme of BILLI system. (b) The red arrow indicates the two large elliptical mirror inside their precision motorized turning mount (opened). The box behind the arrow contains the lasers and telescope.

The transmission subsystem is based on a double grating dye-laser optically pumped by an injection seeded Nd:YAG laser (powerful, tunable, and narrow-linewidth) that also outputs the second harmonic that is used to pump a difference frequency mixing and optical parametric amplifier operating in NIR band. Tm, Ho:YLF, and fiber lasers were discarded mainly for their limited tunability (few tens of nanometers) that can limit the access to choose the best absorption line. An optical parametric oscillator could also be a good choice, but our experience shows that they tend to be quite delicate and not easy to deploy in the harsh environment near degassing craters.[6]

Instead, the receiver subsystem is based on a telescope, a detector, and an analogical to digital converter. More details concerning the mode of operation of the BILLI system are reported in previous works.[3–8] The specifications of the system are shown in Table 1.[6]

It is well known, CO_2 absorbs in the 15, 4.2, 2.1, and 1.6 μm bands (in order of decreasing strength).[4] Unfortunately, in the first two bands, viable lasers are not available and atmospheric backscattering is rather low, so the 2.1 band has been chosen for CO_2 detection.[6] Nevertheless, the DIAL measurement of CO_2 remains a difficult task because the absorption lines are narrow and weak.[4]

Furthermore, with respect to previous experiments,[3–5] during the experimental campaign of Stromboli, the operative wavelengths were slightly changed (see Table 1). This reduced the differential absorption cross-section of carbon dioxide ($\Delta\sigma$), thus allowing the laser beam to reach longer ranges.

Summarizing, the main characteristics of the BILLI DIAL system are the following:

- the system is able to explore the atmosphere in both vertical and horizontal directions;
- each LiDAR profile is obtained averaging 50 shots ON and OFF (interlaced between them with $t_{\text{shift}} = 0.1$ s);
- the temporal resolution between laser shots (Δt) is equal to 10 ns, corresponding to $\Delta R = \pm 1.5$ m;
- a concentration profile is obtained (10 s) by a couple of LiDAR signals (ON and OFF) using the newly designed mathematical technique explicitly developed for this application;

Table 1 Main specifications of the BILLI DIAL system during the Stromboli volcano field campaign.

Transmitter	Pulse energy	25 mJ
	Pulse duration	8 ns
	Repetition rate	10 Hz
	Wavelengths	ON: 2009.537 nm, OFF: 2008.484 nm
	Laser linewidth	0.04 cm^{-1}
	Beam divergence	0.5 mrad
Receiver	Mirror coating	Al
	Clear aperture	300 mm
	Focal length	900 mm
Scanning elliptical mirrors	Mirror coating	Al
	Clear aperture	320 mm × 451 mm
Detector module	Photodiode	InGaAs PIN
	Diameter	1 mm
	Responsivity	1.2 A · W^{-1}
	Gain	$5.1 \cdot 10^4$ V · A^{-1}
	Noise equivalent power	10 pW $Hz^{-1/2}$
	Bandwidth	0 to 10 MHz
Analog-to-digital converter	Dynamic range	14 bit
	Sampling rate	100 MS · s^{-1}

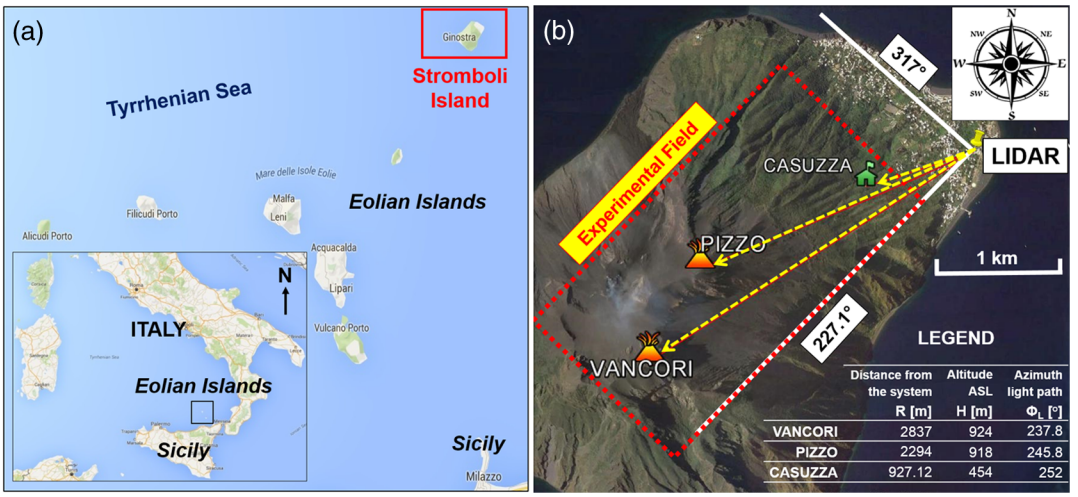

Fig. 2 (a) Map of Eolian Islands—detail of Stromboli volcanic island. (b) Top view of the experimental area and main orographic obstacles.

- starting from LiDAR signals of the same scan, it is possible to retrieve the dispersion map of in-plume CO_2 concentration [ppm] in the investigated area, with an uncertainty varying from 5.8% to 7.4% as a function of the distance from the system;[7]
- knowing the (estimated) plume speed, it is possible to obtain the CO_2 flux (kg/s), with an uncertainty of about 25%;[7]
- starting from LiDAR profiles acquired successively, it is possible to track, as rapidly as possible, the motion of discrete atmospheric particles emitted by the volcanic crater. This allows one to determine the wind speed ($\pm v\,\mathrm{m}\cdot\mathrm{s}^{-1}$).

2.2 *Experimental Setup*

Notwithstanding the harsh environment caused by high humidity and presence of acid vapors and resuspended dust at Stromboli volcano, the BILLI DIAL system operated almost continuously for nearly a week in June 2015.[6,7]

The main goal of the field campaign was to demonstrate the combined determination of carbon dioxide contained in a volcanic plume for early warning of eruptions and the wind speed for rapid tracking of volcanic particles. BILLI was mounted in a truck positioned up to 3 km from the volcanic plume and probed the plume with its laser beam [see Fig. 2(b)], without any risks to authorized personnel.[6,7]

In-situ calibration of the system has been possible due to a fixed reference point: a small building, named "Casuzza" by volcanologists, placed 930 m from the position of the system. This reference point was particularly useful during the data postprocessing step, for converting experimental azimuth angles into real azimuth angles. In fact, once we knew the correct geographical coordinates of this point, it was possible to determine both the exact position of the system and the main topographic obstacles in the investigated area and, therefore, their relative geographic coordinates.

As is shown in Figs. 2(b) and 3, BILLI DIAL system scanned the area of interest in both vertical (elevation angles from 14 to 24 deg) and horizontal planes (azimuth angles from 227 to 317 deg).

For retrieving the wind speed using our system, a set of data (lasting about 90 min) was selected from the morning of June 26, 2015. In Fig. 3, both the azimuth (Φ) and elevation (θ) angles of LiDAR profiles are clearly visible. As will be shown in the next section, this set of data was processed with this correlation method. Finally, experimental results obtained on the field were compared with current values of wind speed and direction acquired by conventional instruments of the nearest weather station near Stromboli [4-m above the sea level (ASL)], 560 m away from the system. This is visible in Fig. 3 (wind speed $\approx 1.38\ \mathrm{m}\cdot\mathrm{s}^{-1}$, wind direction: N-NW).[30]

2.3 *Correlation Function and Wind Speed*

In a LiDAR system, the received light power $P(R)$ comes from the backscattering of the emitted laser pulse by an

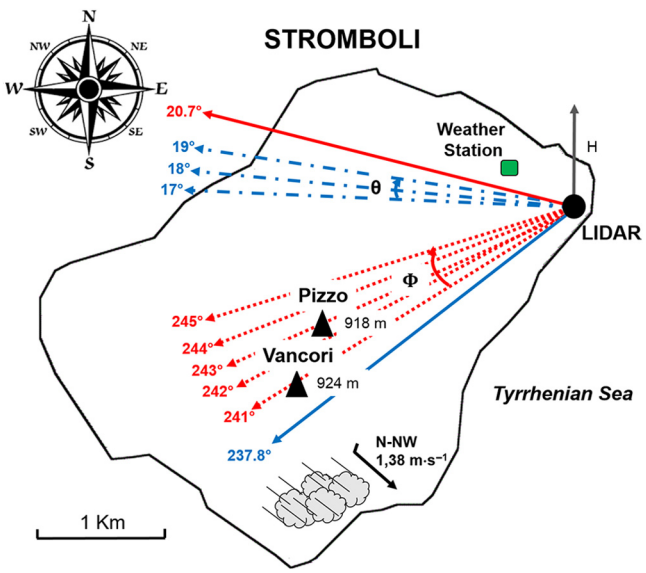

Fig. 3 Setup of the BILLI DIAL system for the measurement of the wind speed. Red lines are relative to the horizontal scan; in particular, the red solid line is the fixed elevation angle, whereas red dashed lines are referred to the variation of azimuth angles. Blue lines are relative to the vertical scan; in particular, the blue solid line is the fixed azimuth angle, whereas blue dashed lines are referred to the variation of the elevation angle.

atmospheric layer at a distance R from the source. The LiDAR equation expresses $P(R)$ in terms of the experimental and atmospheric parameters as follows:[27,28]

$$P(R) = A\xi(R)\frac{E_0}{R^2}\Delta R\beta(R)\exp\left[-2\int_0^R \alpha(R')\mathrm{d}R'\right], \quad (1)$$

where A is the active surface of the receiver, $\xi(R)$ is its detection efficiency, E_0 is the transmitted energy, ΔR is the thickness of the layer, and $\beta(R)$ and $\alpha(R)$ are the backscattering and the extinction coefficients of the atmosphere, respectively. In practice, the range variable R is discrete because of the signal sampling, and an index i is incremented over the spatial bins. The range-corrected signal is normalized by the emitted energy on a shot-per-shot basis to define a normalized signal $S(R_i)$ independent of the energy fluctuation and proportional to the backscattering coefficient:

$$S(R_i) = P(R_i)\frac{R_i^2}{E_0}. \quad (2)$$

The mean normalized signal $\bar{S}(R_i)$ is obtained by averaging N successively recorded individual signals at successive times t_n as follows:

$$\bar{S}(R_i) = \frac{1}{N}\sum_{n=1}^{N} S(R_i, t_n). \quad (3)$$

The information about the shot-per-shot fluctuations of the signals with respect to $\bar{S}(R_i)$ is contained in the fractional deviations:

$$f(R_i, t_n) = \frac{S(R_i, t_n) - \bar{S}(R_i)}{\bar{S}(R_i)}. \quad (4)$$

To determine the displacement of the backscattering inhomogeneities, a cross-correlation function $\rho(L, H_a, H_b)$ is defined with respect to an altitude interval (H_a, H_b) and to a lag value L corresponding to a discrete number of spatial points as follows:

$$\rho(L, H_a, H_b) = \frac{1}{\sigma\sigma_L}\sum_{i=a}^{b}\sum_{n=1}^{N-1} f(R_i, t_n)f(R_{i+L}, t_{n+1}), \quad (5)$$

where

$$\sigma^2 = \sum_{i=a}^{b}\sum_{n=1}^{N-1} f^2(R_i, t_n), \quad (6)$$

$$\sigma_L^2 = \sum_{i=a}^{b}\sum_{n=1}^{N-1} f^2(R_{i+L}, t_{n+1}), \quad (7)$$

$$z_i = R_i \sin\theta, \quad (8)$$

$$\Delta R = R_{i+1} - R_i, \quad (9)$$

$$\Delta t = t_{n+1} - t_n. \quad (10)$$

The radial wind speed v_R in the altitude interval (H_a, H_b) is determined from the lag value $L_{\max}$ for which the correlation is maximum:

$$v_R = L_{\max}\frac{\Delta R}{\Delta t}. \quad (11)$$

Neglecting the vertical transport, a good assumption in usual atmosphere, the horizontal wind speed is then estimated as follows:

$$v = \frac{v_R \cos\theta}{\cos\Delta\Phi}, \quad (12)$$

where θ is the elevation angle of the telescope and $\Delta\Phi$ is the difference in the azimuthal orientation of the wind vector Φ_v and of the light path Φ_L. In this particular case, Φ_v is equal to the wind direction angle (≈315 deg, with respect to the north) and Φ_L is the azimuth angle of the laser beam with respect to the north (varying from 237.8 deg for the vertical scan and between 241 and 245 deg for the horizontal scan).

3 Results and Discussions

Results reported in this paper are relative to the data acquired between June 24 and 29, 2015. In particular, the attention was focused on a limited portion of data acquired between 10:21 and 11:46 (local time) on Friday, June 26, 2015. This time interval was chosen for the following reasons:

- The quality and effectiveness of the measurements provided by our system. As is visible in Fig. 4, an example of in-plume CO_2 concentration vertical scan, extrapolated from the session performed between 11:21 and 11:46 (local time), clearly shows the complete time evolution of this chemical species as a function of time (expressed in seconds) and altitude (in meters) of the laser beam.
- The presence of both vertical and horizontal scan, as already mentioned in Fig. 3. This was extremely useful for validating our processing method in two different situations.
- Moreover, a limited time interval was specifically chosen, to test the efficiency and the rapidity of our technique for wind speed tracking.
- The absence of precipitation and other adverse climatic events, as observed in the field.

Even though most of the LiDAR returns were acquired with a vertical orientation of the optical path, no vertical wind could be detected because the vertical wind speed is very small and below the sensitivity of our current system configuration.

Following the procedure reported in Sec. 2.3, for the evaluation of the wind speed, it is necessary to first retrieve the fractional deviation of the signals.

For example, the fractional deviations of the dataset named as region B, acquired with a beam axis elevation from 17.7 to 18.02 deg and a fixed azimuth angle of 237.8 deg, are shown in Fig. 5. The whole sample, of ∼1.5 min in duration, is composed of nine mean LiDAR returns. This dataset was used to illustrate the time evolution of in-plume spatial aerosols inhomogeneities, as a function of altitude and elevation angle, and to explain the steps of the analysis presented below, if not otherwise stated.

As seen in Fig. 5, successive fractional deviations at the OFF wavelength (this wavelength was chosen because it was

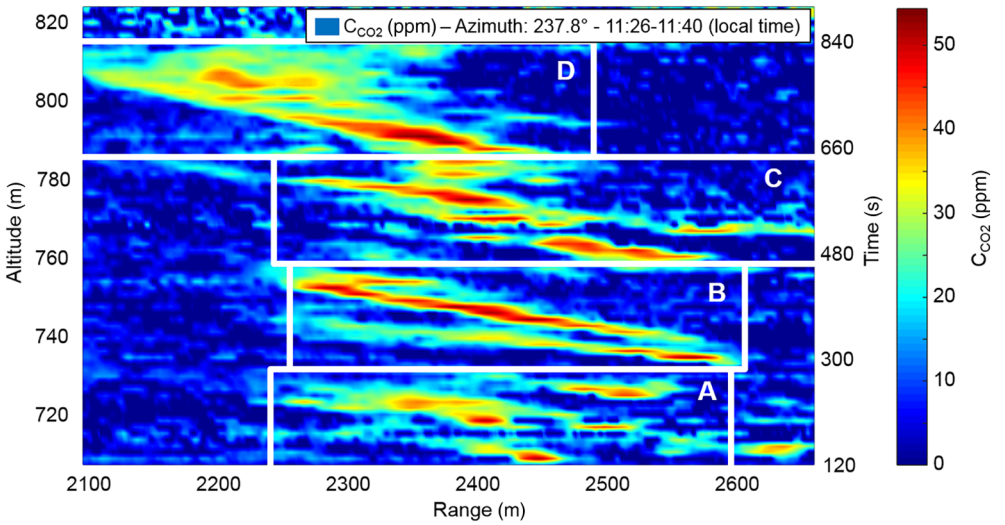

Fig. 4 In-plume CO_2 concentration map acquired June 26, 2015, at Stromboli. Tomography reported above was extrapolated from the measurement session performed between 11:21 and 11:46 (local time), and it represents a dataset acquired as a single group of measurements slowly stepping up in elevation angle (from 16.8 to 20 deg) over the course of about 14 min (from the total session duration of about 25 min) since, during that time, the plume displacement is extremely clear. Carbon dioxide concentration varies as a function of increasing altitude (on the left of the map) and the time of acquisition (on the right). Regions highlighted with white boxes and named as A, B, C, and D are posited to be the same set of scatterers being tracked over time. Therefore, they represent a useful example for summarizing the time evolution of inhomogeneities relative to the volcanic plume. To appreciate these displacements, it is necessary to specify that particles detected in region A need a certain amount of time for moving to the regions B (about 3 min), C (about 6 min), and D (about 9 min). As observed in the field, these movements were mainly due to the presence of wind blowing from the north–northwest.

less absorbed) show the rapid displacement of the main peak of backscattered signal. This peak is highlighted in red, and, starting our analysis from the first profile (no. 26), it is possible to notice its movement from bottom to top of the figure, with increases of the beam axis elevation and acquisition time.

This evolution was interpreted as global due to an average $0.6\ \mathrm{m}\cdot\mathrm{s}^{-1}$ wind component at an average altitude of 747 m above the LiDAR location.

As already mentioned in Ref. 27, when LiDAR signals are averaged over larger spatiotemporal intervals, the determination of the fractional deviations is more accurate but their amplitude is reduced and the resolution of the wind profile is lowered. For these reasons, the LiDAR returns were acquired with a high spatiotemporal resolution ($1.5\ \mathrm{m} \times 12\ \mathrm{s}$), and limited sample sizes (10 LiDAR profiles or less) were chosen. These facts ensured that the measured wind speed remained independent of random inhomogeneities of the backscattering profile.

The second step of our method consists of the calculus of the cross-correlation function. In Fig. 6(a), it is reported an example of the cross-correlation function against the lag value L is reported. This function was extrapolated from the region B (see Fig. 4), selecting intervals (H_a, H_b) of about 20 m in altitude between 737 and 757 m. In this specific case, the maximum value of the cross-correlation function corresponds to $L = -1$. A negative value of lag corresponds to wind blowing toward the LiDAR system's position.

With regard to Fig. 4, it should be noted that no measurements could be extracted above 810 m, where the cross-correlation function was oscillating because of the signal noise.

The third step consists of employing a Gaussian estimator to calculate its mean and standard deviation, and the corresponding curve is superimposed on the data. These values are used as the measured radial wind speed and for the error calculation, respectively. In particular, the latter includes contributions from the statistical fluctuations of the signals.

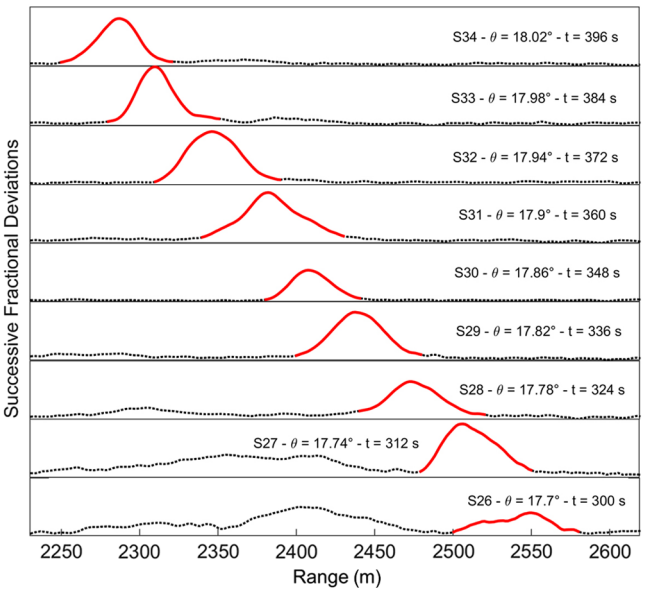

Fig. 5 Successive fractional deviations at the OFF wavelength for $1.5\ \mathrm{m} \times 12\ \mathrm{s}$ spatiotemporal intervals relative to B region of Fig. 4. LiDAR profiles from no. 26 to 34 are reported, and the main peak for each signal is highlighted in red. The displacement of in-plume inhomogeneities (red peaks) as a function of increasing elevation angle and time is clear.

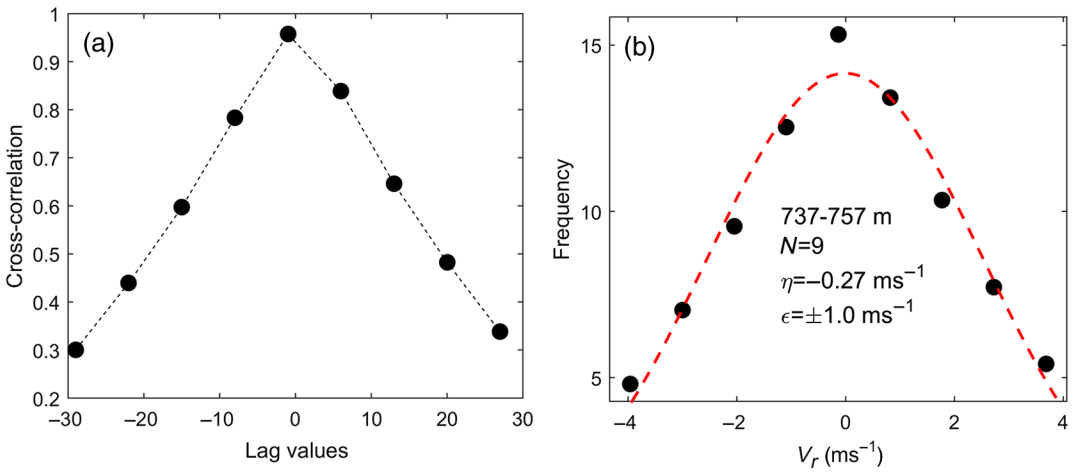

Fig. 6 (a) Cross-correlation function with the highest maximum against the lag value L. (b) Final distribution of the radial wind speed v_R. The altitude interval is defined with respect to the LiDAR level. N stands for the sample size of LiDAR profiles. A Gaussian curve was fitted to the distribution to estimate its mean (η), standard deviation (σ), and standard error (ε). Each graph is relative to the region B of Fig. 4.

Due to this information, the standard error value, defined as $\varepsilon = \sigma/\sqrt{N}$,[31] was determined to be $\varepsilon = \pm 1.0\ \mathrm{m \cdot s^{-1}}$ for region B. As shown in Fig. 6(b), the variable v_R was introduced to show the evolution of the cross-correlation against the radial wind speed, rather than the lag value.

It should be noted that the radial component of the wind speed (v_R) was determined from the radial displacement that occurred to aerosol inhomogeneities as a function of the laser beam elevation angle.

Finally, the last step consists of measuring the horizontal component, obtained by measuring the speed of volcanic particles.

In fact, taking into account the angular difference ($\Delta\Phi$) between the wind direction, with respect to the line-of-sight (LoS) of the laser beam, it is possible to deduce the horizontal wind speed (v), as already shown in Eq. (12) (see Sec. 2.3). For more details about wind components, see Fig. 7.

An example of a vertical wind speed profile is visible in Fig. 8. This graph is relative to the scan carried out between 11:21 a.m. and 11:46 a.m. of June 26, 2015.

Figure 8 shows that reconstructed values of wind speed fluctuate as a function of the altitude. This fact was confirmed by field observations since, during the same hour, there were several variations of wind speed and direction.

Considering the dataset previously mentioned in Fig. 8, the mean value of the wind speed is about $1.3\ \mathrm{m \cdot s^{-1}}$. Moreover, it is possible to notice that our measures are affected by a high uncertainty level. In fact, the weighted mean standard error is globally equal to $\pm 0.52\ \mathrm{m \cdot s^{-1}}$ for the same interval. This was particularly due to the presence of wind blowing in a perpendicular direction with respect to the system location. This is the worst observing condition for the tracking of the wind. In fact, we retrieved the smaller wind speed component along the LoS of the laser beam.

Further results retrieved from the other scan, performed in the same measurement session, confirmed the trend previously stated. In particular, average values of wind speeds and uncertainties were found to be consistent with the ones mentioned in Fig. 8. They are equal to $0.85 \pm 0.47\ \mathrm{m \cdot s^{-1}}$, for the vertical scan performed from the 10:57 to 11:20 (local time) and $1.15 \pm 0.21\ \mathrm{m \cdot s^{-1}}$, for the horizontal scan performed from the 10:21 to 10:57 (local time).

The global weighted average value of wind speed was finally found equal to $1.1 \pm 0.4\ \mathrm{m \cdot s^{-1}}$, for the whole measurement session.

In addition to this, it is evident that wind speed values, observed by conventional instruments ($1.38\ \mathrm{m \cdot s^{-1}}$), are slightly different from our results. Unfortunately, no real-time wind profiler was available at the moment of the campaign for a direct comparison with the LiDAR data. Therefore, as already stressed in Sec. 2.2, the value reported in

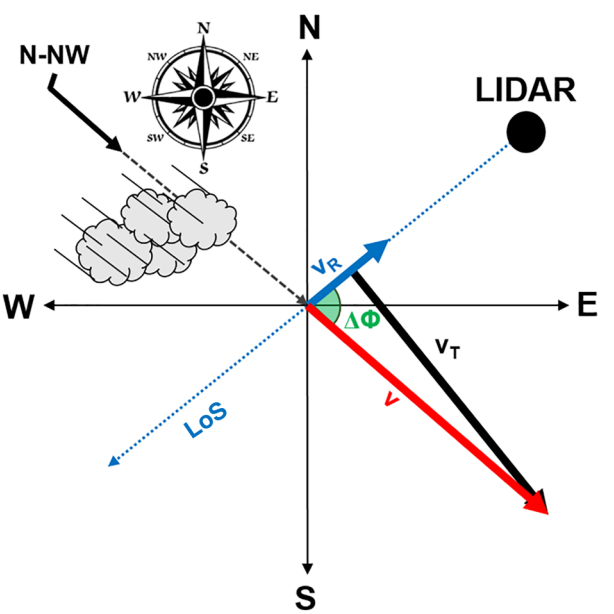

Fig. 7 Top view of a compass rose scheme, useful for wind speed retrieval. Above are reported the LiDAR position, its LoS, and the wind direction (N-NW), retrieved by conventional instruments during the campaign. Moreover, the radial component of wind speed (v_R, in blue), its perpendicular component (v_T, in black), the horizontal wind speed (v, in red), and the angular difference between the azimuthal orientation of the wind vector and of the light path ($\Delta\Phi$, in green) are highlighted with different colors.

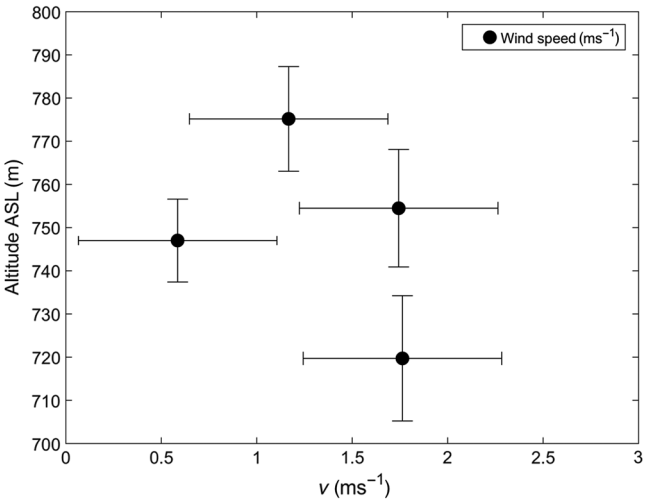

Fig. 8 Vertical wind profile retrieved by LiDAR from 11:26 to 11:46 (local time) of June 26, 2015. The *x*-axis errorbar is the weighted average standard error of wind speed, retrieved during the previous mentioned dataset. That value is equal to $\pm 0.52\ \mathrm{m \cdot s^{-1}}$. Instead, the errorbar on the *y*-axis represents the altitude halfwidth between adjacent regions (A, B, C, and D) previously shown in Fig. 4.

Fig. 3 was retrieved at the nearest weather station located on the island. A six-hour average of weather parameters was acquired 4 m ASL and not at the same height of the laser beam pointing. Therefore, information about wind speed and direction measured by conventional instruments, and reported in this work, can only provide an idea of the weather conditions that occurred at Stromboli during our experimental campaign.

For these reasons, it is not surprising to observe experimentally retrieved values of wind speed lower than the ones acquired by conventional instruments and reported in Fig. 3.

However, comparing experimental results with the ones acquired at the Stromboli weather station, it is possible to notice that they are in agreement within the limits of observed error bounds. In terms of absolute value, the discrepancy between average values of wind speed retrieved by BILLI and the conventional weather station is globally equal to a 25% bias, even though our measurement error is greater, with an uncertainty estimated to be approximately 38% of the measured mean wind speed.

The discrepancies between LiDAR and conventional acquisitions highlight the limits of our system for the wind speed tracking:

- The first limit is represented by the current simple configuration with only one laser beam. This fact limits the performance to a radial measurement along the laser beam LoS, carrying out only one-dimensional measurements. Similarly to sodars or radars,[15,32] a solution to this problem (to obtain 3-D information) could be the implementation of a multibeam configuration, such as the "triple-beam sounding" technique.[15,25] Alternatively, as already suggested,[27] it is possible to implement a fast rotating mirror (by maintaining the single beam configuration) to reconstruct the three component of the wind field. Unfortunately, both solutions still seem to be technologically difficult to apply (and to manage) with the present configuration. In particular, in the second option, the considerable weight of the current scan mirrors ($\approx$20 kg) has to be taken into account. For these reasons, even though these solutions could significantly improve the wind measurement, these improvements are not expected to be applied to the system due to technical and economic issues.
- The second limit is represented by the high uncertainty level that affects our experimental results. This fact is largely expected since the system was not originally conceived for the wind speed tracking. To reduce the inaccuracy of our measurements, a possible solution could be to increase the laser beam energy output. In this way, an improvement of the signal-to-noise ratio is expected.

However, although our system is less accurate than coherent LiDARs,[26] its measurement error is of the same order of other single laser beam instruments[21] and of sodar systems.[32] Furthermore, intercomparisons between instruments of different kinds currently show discrepancies of the order of 0.1 to 2 $\mathrm{m \cdot s^{-1}}$, as shown in Refs. 32–34.

Despite the evident limits of the current system configuration and the (strong) assumptions made here (the presence of vertical transport has been neglected and it has been considered a wind blowing, on average, from N-NW direction during the analyzed measurement session),[30] the information provided is interesting within the context of modeling studies of the spatiotemporal evolution of aerosols and particles in the atmosphere.

Therefore, once we know the wind direction from in-field observations, the horizontal wind component reconstructed from a radial measurement can be used, for example, to provide a rapid means of tracking volcanic ash to improve air traffic security.

The real advantage of the method proposed in this work is that it is possible to retrieve the wind speed with only the addition of further data processing that simultaneously yields in-plume CO_2 concentrations. Our system was explicitly developed for the monitoring of this trace gas as a precursor of volcanic eruptions, and it is possible to obtain a broader set of information about volcanic plume concentration and dispersion without additional costs.

4 Conclusions

In this paper, a mathematical method for the rapid tracking of wind speed using a newly designed DIAL system was presented.

To test the performance of the system, an experimental campaign was carried out at the Stromboli volcano island, with the main goal of performing a combined detection of the exceedance of in-plume CO_2 concentration and the wind speed. Therefore, the main advantage was the retrieval of some weather information with only a further data processing routine and without additional costs.

As already stated in previous work,[6] carbon dioxide was continuously monitored from June 24 to June 29, 2015, since it is considered a precursor gas of volcanic eruptions. Instead, in this work, the first results concerning the wind speed profiling were shown. These results were obtained applying the point correlation method to a limited set of data, with a high spatiotemporal resolution, acquired during the morning of June 26.

Although this is not the first time that the previous cited procedure has been successfully implemented, it should be noted that the retrieval of the wind speed can be extremely useful. In particular, in proximity of an active volcanic region, in order to track the drift of volcanic particles. The knowledge of this information, in combination with CO_2 profiles, could be crucial for providing a precocious alert to population and for adopting rapid and effective countermeasures against eruptions and their deleterious effects on the environment. Once we know the wind direction, an application of great interest for local authorities could be the predictions of volcanic ash displacement due to the presence of wind. This could avoid air travel disruption, improving air traffic security and minimizing the socioeconomic impact of volcanic eruptions.

The authors are conscious that further efforts are needed to improve the system performances and that, in the present configuration, the system is able to perform only one-dimensional measurements of wind speed with high uncertainty. Nonetheless, the results presented in this work are quite consistent with respect to conventional meteorological acquisitions and sufficiently promising if considered in combination with in-plume CO_2 concentration dispersion maps. This proves the ability of the system to provide rapid predictions of wind speed with a precision comparable to that of other stand-alone fixed-beam correlation LiDARs.

In the near future, once technical and economic problems are overcome, it will be desirable and useful to apply this system for continuous monitoring of volcanic hazard zones. This could represent a valuable option for long-term volcano monitoring and for the air traffic safety.

Acknowledgments

The authors are grateful to ENEA, in general, and Aldo Pizzuto, Roberta Fantoni and Antonio Palucci, in particular, for constant encouragement. The support from the ERC project BRIDGE, Grant No. 305377, is gratefully acknowledged.

References

1. "How do volcanoes affect the climate?" The Guardian, London, United Kingdom, 2011, https://www.theguardian.com/environment/2011/feb/09/volcanoes-climate (1 September 2016).
2. A. Aiuppa et al., "Unusually large magmatic CO_2 gas emissions prior to a basaltic paroxysm," *Geophys. Res. Lett.* **37**(17), L17303 (2010).
3. L. Fiorani et al., "Volcanic CO_2 detection with a DFM/OPA-based LiDAR," *Opt. Lett.* **40**(6), 1034–1036 (2015).
4. L. Fiorani et al., "LiDAR detection of carbon dioxide in volcanic plumes," *Proc. SPIE* **9535**, 95350N (2015).
5. A. Aiuppa et al., "New ground-based LiDAR enables volcanic CO_2 flux measurements," *Sci. Rep.* **5**(13614), 1–12 (2015).
6. L. Fiorani et al., "Early detection of volcanic hazard by LiDAR measurement of carbon dioxide," *Nat. Hazards* **83**, 21–29 (2016).
7. A. Aiuppa et al., "New advances in Dial-LiDAR-based remote sensing of the volcanic CO_2 flux," *Front. Earth Sci.* **5**(15), 1–13 (2017).
8. S. Santoro et al., "Volcanic plume CO_2 flux measurements at Mount Etna by mobile differential absorption LiDAR," *Geosciences* **7**(1), 9 (2017).
9. C. M. Riley, "Tephra," Michigan Technological University Geological & Mining, Engineering & Sciences, 2008, http://www.geo.mtu.edu/volcanoes/hazards/primer/tephra.html (1 September 2016).
10. R. Barr, "Iceland's volcanic ash halts flights across Europe," The Guardian, London, United Kingdom, 2010, https://web.archive.org/web/20100423175956/http://www.guardian.co.uk/world/feedarticle/9032564 (1 September 2016).
11. "Flight disruptions cost airlines $1.7bn, says IATA," BBC News, 2010, http://news.bbc.co.uk/2/hi/business/8634147.stm (1 September 2016).
12. "Footage shows Mount Etna spewing lava and ash," BBC News, 2011, http://www.bbc.com/news/world-europe-13381243 (1 September 2016).
13. "Mount Etna eruption closes airport," BBC News, 2014, http://www.bbc.com/news/world-europe-27869840 (1 September 2016).
14. "Erupting Mount Etna closes Calabria airport," The Local, 2015, http://www.thelocal.it/20151203/erupting-mount-etna-closes-calabria-airport (1 September 2016).
15. V. Kovalev and W. E. Eichenger, *Elastic LiDAR, Theory, Practice and Analysis Methods*, Wiley & Sons, Inc., Hoboken, New Jersey (2004).
16. P. Willan, "Stromboli eruption unleashes tidal wave," The Guardian, London, United Kingdom, 2003, https://www.theguardian.com/world/2003/jan/05/italy.philipwillan (1 September 2016).
17. "Eruzione Stromboli 2007: Cronologia eventi principali e azioni di protezione civile," *Protezione Civile*, 2007, http://www.protezionecivile.gov.it/resources/cms/documents/stromboli_eruzione_2007.pdf (1 September 2016).
18. M. Pistolesi et al., "The 15 March 2007 explosive crisis at Stromboli volcano, Italy: assessing physical parameters through a multidisciplinary approach," *J. Geophys. Res.* **116**(B12), B12206 (2011).
19. C. Weitkamp, *LiDAR Range-Resolved Optical Remote Sensing of the Atmosphere*, Springer, New York (2005).
20. J. W. Bilbro, "Atmospheric laser Doppler velocimetry: an overview," *Opt. Eng.* **19**(4), 194533 (1980).
21. E. W. Eloranta, J. M. Kingm, and J. A. Weinman, "The determination of wind speeds in the boundary layer by monostatic LiDAR," *J. Appl. Meteorol.* **14**(8), 1485–1489 (1975).
22. J. L. Schols and E. W. Eloranta, "Calculation of area-averaged vertical profiles of the horizontal wind speed from volume-imaging LiDAR data," *J. Geophys. Res.* **97**(D17), 18395 (1992).
23. European Parliament, Council of the European Union, "Directive 2006/25/EC of the European parliament and of the council of 5 April 2006 on the minimum health and safety requirements regarding the exposure of workers to risks arising from physical agents (artificial optical radiation) (19th individual Directive within the meaning of Article 16(1) of Directive 89/391/EEC)," *Off. J. Eur. Union* **L114**, 38–59 (2006).
24. V. E. Derr and C. G. Little, "A comparison of remote sensing of the clear atmosphere by optical, radio, and acoustic radar techniques," *Appl. Opt.* **9**(9), 1976–1992 (1970).
25. I. Kolev, O. Parvanov, and B. Kaprielov, "LiDAR determination of winds by aerosol in homogeneities: motion velocity in the planetary boundary layer," *Appl. Opt.* **27**(12), 2524–2531 (1988).
26. A. K. Piironen and E. W. Eloranta, "Accuracy analysis of wind profiles calculated from volume imaging LiDAR data," *J. Geophys. Res.* **100**(D12), 25559 (1995).
27. L. Fiorani et al., "A combined determination of wind velocities and ozone concentrations for a first measurement of ozone fluxes with a dial instrument during the MEDCAPHOT-TRACE campaign," *Atmos. Environ.* **32**(12), 2151–2159 (1998).
28. L. Fiorani, "Environmental monitoring by laser radar," Chapter 4 in *Lasers and Electro-Optics Research at the Cutting Edge*, S. B. Larkin, Ed., pp. 123–175, Nova Science Publishers Inc., New York (2006).
29. D. Poreh and L. Fiorani, "Software for analyzing and visualizing laser remote sensing (LIDAR) data," *J. Optoelectron. Adv. Mater.* **12**(5), 1231–1236 (2010).
30. "Previsioni meteorologiche per Stromboli (ME)," Aeronautica Militare, Centro Nazionale di Meteorologia e Climatologia Aeronautica, 2015, http://www.meteoam.it/ta/previsione/893/stromboli (26 June 2015).
31. A. Papoulis and U. Pillai, *Probability, Random Variables and Stochastic Processes*, 4th ed., McGraw-Hill, New York (2002).
32. S. F. Clifford et al., "Ground-based remote profiling in atmospheric studies: an overview," *Proc. IEEE* **82**(3), 313–355 (1994).
33. B. D. Belan et al., "Intercomparison of laser radar and radiosonde techniques of measuring wind speed vector," *Atmos. Oceanic Opt.* **4**(10), 746–749 (1991).
34. W. P. Hooper and E. W. Eloranta, "LiDAR measurements of wind in the planetary boundary layer: the method, accuracy and results from joint measurements with radiosonde and kytoon," *J. Appl. Meteorol.* **25**(7), 990–1001 (1986).

Biographies for the authors are not available.